AIP | APL Materials

# Research Update: Relativistic origin of slow electron-hole recombination in hybrid halide perovskite solar cells

Pooya Azarhoosh, Scott McKechnie, Jarvist M. Frost, Aron Walsh, and Mark van Schilfgaarde

Citation: APL Mater. **4**, 091501 (2016); doi: 10.1063/1.4955028
View online: http://dx.doi.org/10.1063/1.4955028
View Table of Contents: http://scitation.aip.org/content/aip/journal/aplmater/4/9?ver=pdfcov
Published by the AIP Publishing



# Research Update: Relativistic origin of slow electron-hole recombination in hybrid halide perovskite solar cells

Pooya Azarhoosh,[1] Scott McKechnie,[1] Jarvist M. Frost,[2] Aron Walsh,[2,3] and Mark van Schilfgaarde[1,a]

[1]*Department of Physics, Kings College London, London WC2R 2LS, United Kingdom*
[2]*Centre for Sustainable Chemical Technologies and Department of Chemistry, University of Bath, Claverton Down, Bath BA2 7AY, United Kingdom*
[3]*Global E[3] Institute and Department of Materials Science and Engineering, Yonsei University, Seoul 120-749, South Korea*

(Received 11 April 2016; accepted 14 June 2016; published online 21 July 2016)

The hybrid perovskite $CH_3NH_3PbI_3$ (MAPI) exhibits long minority-carrier lifetimes and diffusion lengths. We show that slow recombination originates from a spin-split indirect-gap. Large internal electric fields act on spin-orbit-coupled band extrema, shifting band-edges to inequivalent wavevectors, making the fundamental gap indirect. From a description of photoluminescence within the quasiparticle self-consistent *GW* approximation for MAPI, CdTe, and GaAs, we predict carrier lifetime as a function of light intensity and temperature. At operating conditions we find radiative recombination in MAPI is reduced by a factor of more than 350 compared to direct gap behavior. The indirect gap is retained with dynamic disorder.  [http://dx.doi.org/10.1063/1.4955028]

Metal-organic perovskite solar cells, $CH_3NH_3PbI_3$ (MAPI) in particular, have attracted much recent attention because of their high power conversion efficiency and potential low cost. The material exhibits strong absorptivity characteristic of a direct-gap semiconductor, with the slow radiative recombination characteristic of an indirect-gap semiconductor. The minority carrier diffusion length considerably exceeds the material thickness required for complete solar capture. As such, internal quantum efficiencies approach 100%.[1] Power conversion efficiencies as high as 21% have been reported.[2] The constituent elements are abundant and efficient devices can be made with solution processing methods which offer the potential for low-cost and large scale production. MAPI is thus perhaps the first competitive realization of a "third generation" solar cell.[3]

Minority carrier recombination lifetimes of tens of microseconds are reported in MAPI by time-resolved photoluminescent (TRPL) spectroscopy and other methods.[4–6] Such long lifetimes are found in high-quality samples of crystalline silicon, the archetype indirect-gap semiconductor. A variety of trap-based models have been used to interpret the TRPL data.[6,7] These models suggest that the long lifetimes are due to immobilization of charges in traps. However, samples (both single- and poly-crystalline) with trap density differences of the order $10^5$ have lifetime variations of only an order of magnitude. This suggests that lifetime is weakly correlated with measured trap density. Further, longer lifetimes are observed in low trap-density single-crystal samples.

We show that the observed slow radiative recombination is an *intrinsic property* of MAPI due to the details of the electronic band structure. We formulate the recombination rate in the framework of the quasiparticle self-consistent *GW* (QS*GW*) approximation. A spin-split indirect-gap is formed. Assuming charge carriers thermalize rapidly within a band, we calculate recombination as a function of charge density (illumination intensity) and temperature. With low doping density and solar illumination intensities, the material exhibits an indirect-gap. We show that under operating solar

[a]Electronic mail: mark.van_schilfgaarde@kcl.ac.uk

 

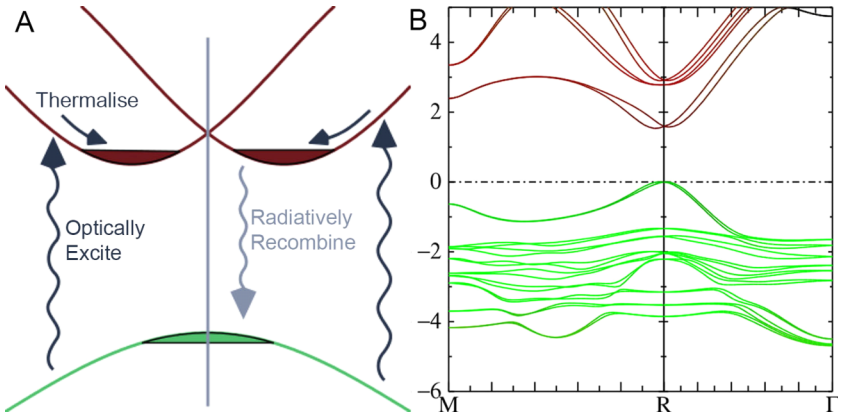


FIG. 1. Electronic band structure of $CH_3NH_3PbI_3$. (a) schematic of absorption and recombination processes. The conduction bands (red) are split around $R$, as opposed to conventional direct-gap semiconductors, where there is a single minimum. Photon absorption (dark grey arrows) generate electron-hole pairs, which quickly thermalize to their respective band edges (dark gray arrows) creating a quasi-equilibrium distribution of carriers (red and green). The excess electrons and hole populations can recombine, creating a photon in the process (light grey arrow). Without phonon assist the transitions must be vertical, as shown. If the electron and hole populations are small, the volume of overlapping $k$ space between the red and green distributions becomes exponentially small in $1/k_BT$, while in CdTe and GaAs the two populations occupy the same phase space for any concentration. (b) QS$GW$ band structure for a section of the $M$–$R$–Γ lines. There is a significant splitting of the conduction band near $R$ ($E \sim 1.75$ eV), and a much smaller splitting of the valence band, near ($E = 0$).

cell conditions, radiative recombination rate is suppressed by over 350 fold; moreover, it varies in an anomalous manner, increasing rapidly with temperature, and illumination intensity and doping. This is in contra-distinction to semiconductors such as CdTe or GaAs, whose recombination properties are also calculated.

For crystals without inversion symmetry, spin-orbit coupling (SOC) splits spin-degenerate levels in non-magnetic systems. In MAPI, significant local electric fields, acting on the large SOC contribution from the heavy lead atom, generate a significant shift in the spin-degenerate conduction band minimum of Pb 6$p$ character. This minimum splits into a pair of minima antipodal to the original point,[8] causing the gap to become slightly indirect (Fig. 1). We investigate the effect of dynamic disorder on this spin splitting. Our initial model is a single unit cell, with an infinite array of aligned organic moieties. In reality, the organic moiety rotates on a picosecond time scale at room temperature.[9–12] We sample molecular dynamics realizations of a disordered supercell. In spite of the disorder, the spin-split indirect-gap is not only present but *enhanced*.

The band splitting is a robust property of the material in working solar cells that suppresses radiative recombination of minority charge carriers, enhancing the photovoltaic action. Two recent studies have noted the importance of the formation of an indirect band gap on the recombination rate of MAPI.[13,14] In Ref. 13, an indirect gap was observed for certain molecular orientations. In Ref. 14, the indirect band gap is recognized as the result of Rashba splitting, leading to a mismatch in both momentum and spin. While their work emphasizes spin mismatch, we believe that the momentum-mismatch dominates device performance as the valence bands are only slightly split, and geminate recombination is likely to be a minor process.

In this letter, we report the recombination rate with spin-orbit coupling included in the Hamiltonian, thus directly treating both spin and momentum mismatch. To our knowledge, the only comparable calculation of radiative recombination was by Filippetti *et al.*[22] where the rate was calculated from density-functional theory without the spin-orbit coupling that is essential for both momentum and spin mismatch.

Above 162 K, MAPI undergoes a continuous transition from a tetragonal to a pseudocubic structure.[10] At room temperature the tetragonal distortion is small, $c/2a \approx 1.01$. The organic moiety in MAPI has a relatively low barrier to rotation[15] and rotates at room temperature in a quasi-random fashion. On average the structure can be considered to be cubic.[9–11] We initially construct a model with a single formula unit of $CH_3NH_3PbI_3$. We orient the organic moiety along [100], [110], and

[111], where local potential energy minima are found, which generate three structures representative of the disordered system.

In the absence of spin-orbit coupling the valence band maximum (VBM) and conduction band minimum (CBM) $k_{\min}$ lie at the $\langle 111 \rangle$ $R$ point.[8,16] The former consists mainly of I $5p$ character, the latter mainly Pb $6p$. The degeneracy of both extrema is split and displaced by spin-orbit coupling ($\langle \xi(r) \rangle \mathbf{L} \cdot \mathbf{S}$), which originates near the atomic cores where $\xi(r)$ is large (Fig. 1). $\langle \xi \rangle$ scales approximately as $Z^2$.

With Pb being so heavy ($Z = 82$), $\langle \xi \rangle \mathbf{L} \cdot \mathbf{S}$ strongly affects the lead $6p$ conduction band, spin-splitting the minima into a pair of distinct states offset from R (Fig. 1). The iodine $5p$ valence band is affected to a lesser extent ($Z = 53$), the spin-split displacement is small, resulting in a flattened region in reciprocal space due to the overlapping minima. The spin-orbit coupling narrows the band gap by ~1 eV. The spin splitting is linear in $k$, in contrast to typical semiconductors where it varies as $k^3$. The band gap thus becomes slightly indirect. The direct band gap $E_0$ remains at $R$ and is 75 meV larger than the indirect gap.

The joint density-of-states (JDOS), relevant for absorption, differs from its direct-gap values in only a small energy range around $E_0$. The flattened valence band contributes to a large density of states available for optical transition at the direct-gap. Thus *absorption* is only slightly affected by the spin-splitting: MAPI absorbs solar radiation as though it were a direct-gap semiconductor. However, *radiative recombination* is dramatically suppressed. This is extremely unusual for a solar cell material, where typically emission and absorption are the direct reverse of one another. Photoexcited electrons (holes) rapidly thermalize to a small region of $k$ space centered at the conduction (valence) band edges. The asymmetry in $k_{\min}^{\mathrm{CBM}}$ and $k_{\min}^{\mathrm{VBM}}$ means that there is a low joint density-of-states of the thermalized minority carriers. Direct ($k$ conserving) recombination is thereby reduced.

Higher temperature leads to greater thermal broadening and a larger overlap in the joint density-of-states, increasing radiative recombination. High density of photogenerated charges (or extrinsic charge carrier doping) fills the small pockets at the CBM. Radiative recombination increases critically, reverting to direct-gap semiconductor behaviour. This property is *intrinsic* to the material; no defect or trap states are needed to explain why radiative recombination is suppressed at low photon flux but increase dramatically at high photon flux. There is some evidence for such behaviour: carrier lifetimes demonstrate a sharp fall at moderate injection densities.[7]

Here we formulate an *ab initio* theory for radiative recombination within the QS*GW* approximation.[17] QS*GW* is parameter free. In *sp* semiconductors a wide range of electronic properties are uniformly well described,[18] including splitting from the Dresselhaus terms.[19] Few fully *ab initio* formulations of radiative recombination have been reported.[20] Calculations using the van Roosbroeck-Shockley relation with experimental[21] and theoretical[22] absorption coefficients have been published. We directly calculate the recombination rate without model parameters, adapting the standard theory of dielectric response to non-equilibrium carrier populations.

The recombination dynamics of carriers within the bulk of an intrinsic semiconductor ($n = p$) can often be accurately described by a third-order rate equation

$$\frac{dn}{dt} = G - n\mathrm{A} - n^2\mathrm{B} - n^3\mathrm{C}. \tag{1}$$

Here $n$ is the density of excited carriers and $G$ is a source term describing constant photogeneration of carriers.[23] These parameters are often fit to experimental transient data across a large range of laser fluences and thus carrier densities.[24] An implicit assumption is that these coefficients do not vary across the carrier density regime experimentally accessed. A is related to the one-body non-radiative carrier recombination, which proceeds through crystal defect levels as intermediate states. We are concerned with intrinsic recombination and do not consider this extrinsic process. C is the three-body Auger recombination coefficient. This has been calculated in a *GW* framework[25] but it becomes important under strongly non-equilibrium carrier populations and we omit it here. The two-body coefficient B describes radiative recombination of free carriers and is intimately connected with both absorption and emission. Photo-generated carriers thermalize to the band edges on a picosecond time scale,[26] which is fast compared to the radiative recombination time (ns to $\mu$s).

We will assume that photoexcited carriers thermalize instantaneously within a band to form quasi-equilibrium Fermi-Dirac distributions of electrons and holes. Thus the occupation probability of an excited electron $c$ is given by $f_c = \left(\exp[(E_c - E_c^F)/k_BT] - 1\right)^{-1}$, where $E_c - E_c^F$ is the excitation energy relative to the electron quasi-Fermi level. The corresponding distribution $f_v$ for excited holes is the same form, substituting $E_c - E_c^F \rightarrow E_v - E_v^F$. In practice, we specify $T$, and electron and hole populations $n$ and $p$. From the QS$GW$ band structure we can calculate the density of states and so determine $E_c^F$ and $E_v^F$ from $n$ and $p$.

To establish that QS$GW$ can reliably predict the photoluminescent process, we compute B for the benchmark materials GaAs and CdTe. This both validates the method developed here and serves as points of comparison to MAPI.

Under solar intensities a small population of electrons (holes) is excited to the conduction (valence) band (Fig. 1). This density is relatively small for an operating solar cell ($\sim 10^{17}$ cm$^{-3}$). Only a small area of $k$ space near the band edges is utilized by photo-excited charge carriers. Numerically, this necessitates a fine $k$ mesh to adequately sample the near regions of the band minima. Some additional modest approximations are necessary to make the calculation tractable. We neglect local fields and use the independent-particle (time-dependent Hartree) approximation. This approximation misses the Wannier excitons below the band edge, but they are very shallow.[27,28] If the potential is local,

$$\epsilon(\omega) = \sum_{\mathbf{k}cv} \epsilon_{\mathbf{k}cv}(\omega) \tag{2}$$

$$\mathrm{Im}\, \epsilon_{\mathbf{k}cv}(\omega) = \frac{1}{\hbar}\left(\frac{2\pi e}{m\omega}\right)^2 |P_{\mathbf{k}cv}|^2 f_c(1 - f_v)\delta(\omega - \omega_{\mathbf{k}cv}). \tag{3}$$

$\epsilon_{\mathbf{k}cv}$ resolves $\epsilon$ into individual electron-hole excitations between Bloch states $v$ and $c$; $\hbar\omega_{\mathbf{k}cv} = E_c(\mathbf{k}) - E_v(\mathbf{k})$ is the excitation energy of the $cv$ pair. The photons couple $c$ to $v$, which for direct transitions simplifies to a matrix element of the momentum operator $P_{\mathbf{k}cv}$. We omit phonon-assisted indirect transitions that do not conserve $k$ because they are weaker, higher-order processes. As written Eq. (3) is approximate because the QS$GW$ potential is non-local. However, for transitions close to $E_0$ the effect of non-locality can be described by a scaling of $P_{\mathbf{k}cv}$.[29] Further details of the theory are given in the supplementary material.[30]

By resolving $\mathrm{Im}\,\epsilon$ into individual pair contributions, the transition rate (Einstein coefficient) $A_{\mathbf{k}cv}$ between a $cv$ pair can be readily identified,

$$A_{\mathbf{k}cv} = \frac{n_r e^2 \omega_{\mathbf{k}cv} |P_{\mathbf{k}cv}|^2}{\pi\epsilon_0 \hbar c^3 m^2}, \tag{4}$$

and the energy-resolved radiative recombination rate is

$$R_{\mathbf{k}cv}(\omega) = f_c(1 - f_v)A_{\mathbf{k}cv}\delta[\omega - \omega_{\mathbf{k}cv}]. \tag{5}$$

The total emission rate

$$R^{\mathrm{tot}} = \int_0^\infty d\omega \sum_{\mathbf{k}cv} R_{\mathbf{k}cv}(\omega) \tag{6}$$

is conventionally expressed in terms of a carrier density independent recombination lifetime $\tau$ or a B coefficient

$$\tau^{-1} = \mathrm{B}n = R^{\mathrm{tot}}/n. \tag{7}$$

We neglect the scattering processes that eventually lead to thermalization of electrons (holes) during photoluminescence. We adopt the standard approximation in device modeling and assume that recombination is slow compared to the scattering of charge carriers within a band, so a quasi-equilibrium Fermi-Dirac distribution is maintained with a well-defined, band-dependent chemical potential.

B, computed as a function of carrier density for MAPI, CdTe, and GaAs at several temperatures, is shown in Fig. 2. Measured values at room temperature are displayed in Table I. These vary

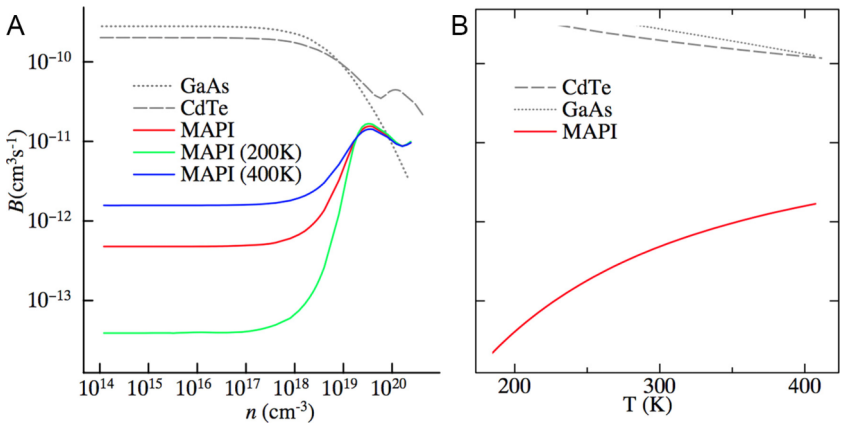


FIG. 2. Radiative recombination coefficient for varying temperature and excitation intensity. (a) Radiative recombination coefficient B in the intrinsic case $n = p$. B for CdTe, GaAs, and MAPI at room temperature, varying photoexcitation density $n$. All have comparable direct band gaps and effective masses. At $n > 10^{18}$ cm$^{-3}$ the MAPI spin-split indirect-gap saturates and the rate of radiative recombination becomes similar in all three materials. Also shown are MAPI calculated at 200 K and 400 K. The effect of the indirect gap becomes more pronounced as $T$ decreases. (b) Temperature dependence of radiative recombination for $n = 10^{16}$ cm$^{-3}$.

widely, presumably owing to the competition of B with other, non-radiative, recombination paths. The presence of these pathways will depend strongly on how the material is fabricated, and so the smallest measured B value is probably the most reliable, and the most directly comparable to our calculations. We calculate B to be more than two orders of magnitude smaller in MAPI than the direct-gap semiconductors CdTe and GaAs, but larger than the fully indirect Si. MAPI resembles an indirect gap semiconductor for radiative carrier recombination, and a direct gap semiconductor for absorption.

The magnitude of B increases as the $k$-space overlap between electron and hole distributions increases. This causes the rate of bimolecular recombination to depend on external parameters in an unusual manner. For example, increasing temperature smears $f_c$ and $f_v$ over a wider band of $k$ for fixed $n$, causing B to increase with $T$. The temperature dependence of B in GaAs and CdTe (Fig. 2) is weaker and of opposite sign. Further, bimolecular recombination will increase abruptly with photoexcited carrier density once the electron pockets begin to fill up and overlap ($n \sim 10^{18}$ cm$^{-3}$ in Fig. 2), in sharp contrast to CdTe and GaAs. Only at high carrier concentrations when a significant fraction of electrons and holes overlap does B in MAPI become comparable to B in CdTe, where it also adopts the conventional behaviour and begins to decrease with increasing $n$. The strong carrier density, and therefore laser-fluence, dependence of B suggests that global fits to time resolved data are not a reliable method to infer B or lifetime from B (Equation (7)). The variation of B with carrier density will make high fluence transients multi-exponential and break the expected relationship between light-emission and carrier-density sensitive experimental probes.

For photoexcitation densities $n < 10^{17}$ cm$^{-3}$ ($n = p$), we find B $\approx 4 \times 10^{-13}$ at room temperature. These are the charge carrier densities relevant for device operation in sunlight. As B is fairly constant below this charge carrier density, we can use Equation (7) to derive a lifetime of order

TABLE I. Experimental and QS*GW* values for B at room temperature, and $n = 10^{17}$ cm$^{-3}$.

| | Expt ($10^{-12}$ cm$^3$ s$^{-1}$) | QS*GW* |
|---|---|---|
| MAPI | See text | 0.49 |
| GaAs[35–37] | 130–1300 | 267 |
| CdTe[38–40] | 100–5100 | 195 |
| Si[41,42] | 0.001–0.01 | |

10-100 $\mu$s. This lifetime is consistent with values reported in the literature for single crystal samples under 1 and 0.1 sun intensity.[4–6]

There are limited temperature dependent TRPL data available. Most data are for polycrystalline films, whereas our results would best be compared to single crystal measurements. Yet it has been observed that the carrier lifetime is highly temperature sensitive at low fluence while being temperature insensitive at high fluence.[6] The increase in minority carrier lifetime with decreasing sample temperature can be directly explained by a contraction of the Fermi-Dirac distribution near the spin-split band minima.

So far we have considered MAPI in an idealized static structure. In reality, the high temperature phase of MAPI is cubic on average only; the dipolar molecules between cages continually rotate, the cages flex and tilt. Second-order Jahn-Teller deformations of the octahedra due to the Pb 6*s* lone pair directly distort the lead iodide bonds, generating local electric fields near the atomic core region where spin-orbit coupling is high. Recent molecular-dynamics simulations by Etienne *et al.*[31] suggest that the conduction band splitting persists in the presence of disorder.

If the material has true inversion symmetry, as MAPI is believed to in the orthorhombic phase below 162 K, no directional electric fields can exist, and so the spin-split indirect-gap should vanish. The rate of radiative recombination should increase, increasing the competition with non-radiative recombination and thus increasing photoluminescent efficiency.

To assess the effect of dynamic disorder we performed *ab-initio* molecular dynamics at 300 K with a $2 \times 2 \times 2$ supercell. Such supercells are able to accurately describe the phonon modes both at the $\Gamma$ point and the Brillouin zone boundary; these $k$-points contain the important low-energy vibrational modes responsible for disorder. We extract 100 realizations, each temporally separated by 2.5 ps, collected after an initial equilibration period. Given the increased computational cost of this larger structure (96 versus 12 atoms), the electronic properties were calculated within the local density approximation (LDA) including spin-orbit coupling. While our intent is to show the qualitative effect of disorder on the magnitude of the spin-split indirect-gap and the effective masses, the LDA results for the ordered cells are in reasonable agreement with QS*GW* (Table II).

Between molecular dynamics snapshots, the spin-split band extrema and effective masses fluctuate. As can be seen from values averaged over the 100 instances (Table II), disorder causes the light effective masses to increase. This may explain the observed reduction in mobility as a function of temperature, in the temperature regime where the organic moieties are increasingly disordered. Surprisingly, the band minima spin-split $k_{\text{min}}$ *also* increases with disorder. This suggests that the cage deformation plays a more important role in generating the directional electric field than the ordering of the moiety dipoles. This is indirectly supported by the success of the formamidinium based perovskites, with smaller dipoles but larger anisotropy.[32,33]

Although the model presented here shows good agreement with experiment, other mechanisms that suppress bimolecular recombination may be operative. In particular, electric fields generated by local ferroelectric domains or defect segregation could separate electrons and holes in *real* space,[15,34] in contrast to the present work, where B is suppressed by separation in *reciprocal* space. Both mechanisms could contribute simultaneously to reduced recombination. We pointed to a

TABLE II. Calculated values of $k_{\text{min}}$ and conduction band effective masses along the three principal axes. LDA results for the molecular dynamics $2\times2\times2$ supercell are the average from one hundred snapshots.

| Structure | Theory | $k_{min}$ (Å $^{-1}$) | $m_1$ | $m_2$ | $m_3$ |
|---|---|---|---|---|---|
| Pseudocubic ⟨100⟩ | QS*GW* | 0.043 | 0.95 | 0.13 | 0.11 |
| Pseudocubic ⟨110⟩ | | 0.055 | 0.13 | 0.11 | 0.11 |
| Pseudocubic ⟨111⟩ | | 0.043 | 0.36 | 0.12 | 0.12 |
| Pseudocubic ⟨100⟩ | LDA | 0.049 | 1.03 | 0.09 | 0.06 |
| Pseudocubic ⟨110⟩ | | 0.057 | 0.08 | 0.07 | 0.06 |
| Pseudocubic ⟨111⟩ | | 0.049 | 0.27 | 0.08 | 0.08 |
| Molecular Dynamics | | 0.105 | 1.02 | 0.60 | 0.42 |

limited body of evidence to support the latter; along these lines it is noteworthy that high power conversion efficiencies have been reported only for lead-based halide perovskites. This is consistent with the spin-split indirect gap picture, as SOC is weaker in lighter elements such as Sn. In principle it is possible to obtain experimental evidence for the direct/indirect-gap picture, with optical probes of the (weakly emissive) indirect gap. Sensitive photoluminescence (PL) or electroluminescence (EL) would probe the emission from this state, absorption can be probed by sensitive external quantum efficiency (EQE) or photo-deflection spectroscopy (PDS). In our idealized structure we predict the splitting to be 75 meV, while in the actual, disordered case it will vary with the disorder.

In summary we have provided a fully *ab initio* relativistic calculation of the hybrid halide perovskite radiative recombination lifetime. We considered only direct recombination, and with electron and hole populations described by a quasi-Fermi level. We have shown that the bimolecular recombination rate is strongly temperature and carrier density sensitive and that the long carrier lifetime and diffusion length are a direct consequence of large relativistic spin-orbit coupling combined with internal electric fields. We suggest that the relevant electric fields are mainly generated by dynamic deformation of the inorganic octahedral cage. The spin-split indirect gap is generated by the Pb lone-pair driven distortions and the Pb spin-orbit coupling of the conduction band. For perovskite alloys, for example, formamidinium/methylammonium/caesium and iodine/bromine, the additional symmetry breaking due to occupational site disorder would be expected to further enhance these effects, which is consistent with their strong photovoltaic action.

The authors thank Jenny Nelson, Thomas Kirchartz, and Keith Butler for useful discussions. The research has been supported by the EPSRC (Grant Nos. EP/K016288/1, EP/M009580/1, and EP/M009602/1), the Royal Society, and the European Research Council (No. 277757). Computational resources were provided by the University of Bath and the EPSRC (Grant No. EP/L000202).

[1] Q. Lin, A. Armin, R. C. R. Nagiri, P. L. Burn, and P. Meredith, Nat. Photonics **9**, 106 (2015).
[2] H. Zhou, Q. Chen, G. Li, S. Luo, T.-B. Song, H.-S. Duan, Z. Hong, J. You, Y. Liu, and Y. Yang, Science **345**, 542 (2014).
[3] M. Green, *Solar Cells: Operating Principles, Technology, and System Applications*, Prentice-Hall Series in Solid State Physical Electronics (Prentice-Hall, 1982).
[4] Q. Dong, Y. Fang, Y. Shao, P. Mulligan, J. Qiu, L. Cao, and J. Huang, Science **347**, 967 (2015).
[5] D. Shi, V. Adinolfi, R. Comin, M. Yuan, E. Alarousu, A. Buin, Y. Chen, S. Hoogland, A. Rothenberger, K. Katsiev, Y. Losovyj, X. Zhang, P. A. Dowben, O. F. Mohammed, E. H. Sargent, and O. M. Bakr, Science **347**, 519 (2015).
[6] S. D. Stranks, V. M. Burlakov, T. Leijtens, J. M. Ball, A. Goriely, and H. J. Snaith, Phys. Rev. Appl. **2**, 034007 (2014).
[7] Y. Yamada, T. Nakamura, M. Endo, A. Wakamiya, and Y. Kanemitsu, J. Am. Chem. Soc. **136**, 11610 (2014).
[8] F. Brivio, K. T. Butler, A. Walsh, and M. van Schilfgaarde, Phys. Rev. B **89**, 155204 (2014).
[9] E. Mosconi, C. Quarti, T. Ivanovska, G. Ruani, and F. De Angelis, Phys. Chem. Chem. Phys. **16**, 16137 (2014).
[10] M. T. Weller, O. J. Weber, P. F. Henry, A. M. Di Pumpo, and T. C. Hansen, Chem. Commun. **51**, 4180 (2015).
[11] A. M. A. Leguy, J. M. Frost, A. P. McMahon, V. G. Sakai, W. Kockelmann, C. Law, X. Li, F. Foglia, A. Walsh, B. C. O'Regan, J. Nelson, J. T. Cabral, and P. R. F. Barnes, Nat. Commun. **6**, 7124 (2015).
[12] A. A. Bakulin, O. Selig, H. J. Bakker, Y. L. Rezus, C. Mller, T. Glaser, R. Lovrincic, Z. Sun, Z. Chen, A. Walsh, J. M. Frost, and T. L. C. Jansen, J. Phys. Chem. Lett. **6**, 3663 (2015).
[13] C. Motta, F. El-Mellouhi, S. Kais, N. Tabet, F. Alharbi, and S. Sanvito, Nat. Commun. **6**, 7026 (2015).
[14] F. Zheng, L. Z. Tan, S. Liu, and A. M. Rappe, Nano Lett. **15**, 7794 (2015).
[15] J. M. Frost, K. T. Butler, F. Brivio, C. H. Hendon, M. van Schilfgaarde, and A. Walsh, Nano Lett. **14**, 2584 (2014).
[16] M. Kim, J. Im, A. J. Freeman, J. Ihm, and H. Jin, Proc. Nat. Am. Soc. **111**, 6900 (2014).
[17] Our implentation was adapted from the original ecalj code at https://github.com/tkotani/ecalj and available at http://www.lmsuite.org/.
[18] M. van Schilfgaarde, T. Kotani, and S. Faleev, Phys. Rev. Lett. **96**, 226402 (2006).
[19] A. N. Chantis, M. van Schilfgaarde, and T. Kotani, Phys. Rev. Lett. **96**, 086405 (2006).
[20] G. Lasher and F. Stern, Phys. Rev. **133**, A553 (1964).
[21] C. Barugkin, J. Cong, T. Duong, S. Rahman, H. T. Nguyen, D. Macdonald, T. P. White, and K. R. Catchpole, J. Phys. Chem. Lett. **6**, 767 (2015).
[22] A. Filippetti, P. Delugas, and A. Mattoni, J. Phys. Chem. C **118**, 24843 (2014).
[23] E. Kioupakis, Q. Yan, D. Steiauf, and C. G. V. de Walle, New J. Phys. **15**, 125006 (2013).
[24] R. L. Milot, G. E. Eperon, H. J. Snaith, M. B. Johnston, and L. M. Herz, Adv. Funct. Mater. **25**, 6218 (2015).
[25] T. Kotani and M. van Schilfgaarde, Phys. Rev. B **81**, 125201 (2010).
[26] M. B. Price, J. Butkus, T. C. Jellicoe, A. Sadhanala, A. Briane, J. E. Halpert, K. Broch, J. M. Hodgkiss, R. H. Friend, and F. Deschler, Nat. Commun. **6**, 8420 (2015).
[27] J. Even, L. Pedesseau, and C. Katan, J. Phys. Chem. C **118**, 11566 (2014).
[28] A. Miyata, A. Mitioglu, P. Plochocka, O. Portugall, J. T.-W. Wang, S. D. Stranks, H. J. Snaith, and R. J. Nicholas, Nat. Phys. **11**, 582 (2015).
[29] R. Del Sole and R. Girlanda, Phys. Rev. B **48**, 11789 (1993).

[30] See supplementary material at http://dx.doi.org/10.1063/1.4955028 for further technical details of the recombination rate model.
[31] T. Etienne, E. Mosconi, and F. D. Angelis, J. Phys. Chem. Lett. **7**, 1638 (2016).
[32] G. E. Eperon, S. D. Stranks, C. Menelaou, M. B. Johnston, L. M. Herz, and H. J. Snaith, Energy Environ. Sci. **7**, 982 (2014).
[33] N. J. Jeon, J. H. Noh, W. S. Yang, Y. C. Kim, S. Ryu, J. Seo, and S. I. Seok, Nature **517**, 476 (2014).
[34] J. Ma and L. W. Wang, Nano Lett. **15**, 248 (2015).
[35] G. W. 't Hooft, Appl. Phys. Lett. **39**, 389 (1981).
[36] P. J. Bishop, M. E. Daniels, B. K. Ridley, and K. Woodbridge, Phys. Rev. B **45**, 6686 (1992).
[37] F. Stern, IEEE J. Quantum Electron. **9**, 290 (1973).
[38] C. H. Swartz, M. Edirisooriya, E. G. LeBlanc, O. C. Noriega, P. A. R. D. Jayathilaka, O. S. Ogedengbe, B. L. Hancock, M. Holtz, T. H. Myers, and K. N. Zaunbrecher, Appl. Phys. Lett. **105**, 222107 (2014).
[39] A. Kirk, M. DiNezza, S. Liu, X. H. Zhao, and Y. H. Zhang, in *39th IEEE Photovoltaic Specialists Conference (PVSC)* (IEEE, 2013), pp. 2515–2517.
[40] X. H. Zhao, M. J. DiNezza, S. Liu, S. Lin, Y. Zhao, and Y. H. Zhang, J. Vac. Sci. Technol. B **32**, 040601 (2014).
[41] T. Trupke, M. A. Green, P. Würfel, P. P. Altermatt, A. Wang, J. Zhao, and R. Corkish, J. Appl. Phys. **94**, 4930 (2003).
[42] W. Gerlach, H. Schlangenotto, and H. Maeder, Phys. Status Solidi A **13**, 277 (1972).